N-[2-(5-bromo-2-chloro-pyrimidin-4-yl)thio)-4-methoxy-phenyl]-4-chlorobenzenesulfonamide: The existence of H-bond and halogen bond interactions assisted supramolecular architecture – A quantum chemical investigation

T.N. Lohith [a], M.K. Hema [a], C.S. Karthik [b,*], S Sandeep [b], L Mallesha [c,*], P Mallu [b], R Jothi Ramalingam [d], M.A. Sridhar [a], Muthusamy Karnan [e], N.K. Lokanath [a]

[a] Department of Studies in Physics, University of Mysore, Manasagangotri, Mysuru 570 006, Karnataka, India
[b] Department of Chemistry, SJCE, JSS Science and Technology University, Mysuru 570 006, Karnataka, India
[c] PG Department of Studies in Chemistry, JSS College of Arts, Commerce and Science, Ooty Road, Mysuru 25, India
[d] Department of Chemistry, College of Science, King Saud University, P.O. Box. 2455, Riyadh 11451, Kingdom of Saudi Arabia
[e] Grassland and Forage division, National Institute of Animal Science, Rural Development Administration, Chungcheongnam-do, Cheonan-si 31000, South Korea

ARTICLE INFO

ABSTRACT

Different types of noncovalent interactions like hydrogen bond and halogen bond are analyzed for the pyrimidine containing sulfonamide derivative. Detailed structural, noncovalent, halogen interactions present in the title compound has been investigated by the single crystal X-ray diffraction study. The compound is crystallized in the triclinic crystal system with the space group $P\bar{1}$. The crystal structure analysis revealed that various N-H...N, N-H...S, C-H...N, and C-H...O interactions are responsible for crystal packing. The different components are connected by a network of hydrogen bonds and halogen...halogen interactions. Also, The Hirshfeld surface analysis were done to validate the interactions quantitatively. The results obtained from *ab initio* calculations described herein reveal a major contribution from the electrostatic interaction on the stability of the systems considered. Beside the electrostatic interaction, the charge-transfer force and the second-order orbital interaction also play an important role in the formation of the title molecule, as suggested by the NBO analysis. The presence of halogen bonds in the molecule has been identified in terms of the QTAIM and NCI analyses, and several linear relationships have been established to provide more insight into halogen bonding interactions.

© 2022 Published by Elsevier B.V.

1. Introduction

Beyond the field of covalent chemistry, there has been a thriving world of supramolecular chemistry, which strives to create very complex chemical systems from components interacting through noncovalent intermolecular forces. In crystal engineering, one of the areas of increasing interest is the examination of supramolecular architecture created via noncovalent interactions. Noncovalent interaction's structure supramolecular materials, allowing for reversible self-assembly, has advantages in production, processing, and recycling [1,2]. Supramolecular chemistry (interactions) also takes its cues from biological molecules like proteins and lipids, as

well as their interactions [3]. The assembly of supramolecular assembly using noncovalent intermolecular interactions such as hydrogen and halogen bonding is well established. Nonconventional hydrogen and halogen bonds have been recognized for 70 years and are generally considered to be weak bonds. While these bonds are well-established as important cooperative intermolecular interactions in the solid state [4].

The halogen bond is a key noncovalent supramolecular interaction that is increasingly drawing significant consideration in the study of protein-ligand complexes [5]. Halogens are found in both inorganic and organic chemistry, where they serve as monodentate or bridging ligands for a wide range of d-block, f-block, and main group metals, as well as being common substituents in a wide range of organic compounds. Halogen atoms are usually found on the periphery of organic molecules, making them suitable candidates for intermolecular interactions. In di-halogens and halocarbons, the potential of halogen atoms to interact effectively with

* Corresponding authors.
  E-mail addresses: csk@jssstuniv.in (C.S. Karthik), mallesha83@gmail.com (L. Mallesha).

electron donors was discovered as early as the 19th century [6]. Halogen bonding is likely the least studied noncovalent interaction, particularly in the solution phase, and its promise in supramolecular chemistry applications is only now being realized [7]. Hydrogen bonding is a powerful tool for constructing dynamic supramolecular structures, and it plays a significant role in biological systems. The great directionality and fidelity of hydrogen bonding make it a popular choice. Individual hydrogen bonds are weak, but a multiple hydrogen bonding array may be more stable and have a substantially higher binding strength [8].

The resulting steric accessibility could make halogenated compounds an appealing target for use in supramolecular chemistry and crystal engineering, where the halogen atoms are directly implicated in the formation of intermolecular interactions [9]. Halogen interaction finds application in various fields like phosphorescent material [10,11], organo catalysis [12,13], drug design [14,15], crystal engineering [16,17] and so on. Due to its wide range of applications as highly directional motifs in supramolecular chemistry, halogen bonding has intrigued attention in recent years. Inforecite of the above discussion, pyrimidine coupled sulfonamide derivative was crystallized, and structure was elucidated using SXRD. The different types of noncovalent interactions like hydrogen bond and halogen bond were investigated in the present work.

2. Materials and methods

All solvents and reagents were purchased from Merck chemicals. Melting range was determined by Veego Melting Point VMP III apparatus. Elemental analyses were recorded on Vario MICRO superuser V1.3.2 Elementar. The FT-IR spectra were recorded using KBr discs on FT-IR Jasco 4100infrared spectrophotometer.1H NMR spectra were recorded on Bruker DRX -500 spectrometer at 400 MHz usingd6-DMSO as solvent and TMS as internal standard. Silica gel column chromatography was performed using Merck7734 silica gel (60–120 mesh) and Merck-made TLC plates.

2.1. Synthesis of N-[2-(5-bromo-2-chloro-pyrimidin-4-yl)thio)-4-methoxy-phenyl]-4-chlorobenzenesulfonamide (3)

The experimental procedure described as per our previous research [18] afforded 3, and the product obtained from 2-(5-bromo-2-chloropyrim-idin-4-ylthio)-4-methoxybenzenamine (1) (3.47 g, 0.01 mol) and 4-chlorobenzenesulfonyl chloride (2) (2.19 g,0.01 mol) as shown in Scheme 1s. The compound 3 is dissolved in ethanol and kept for slow evaporation at ambident temperature for 4 days. FT-IR (KBr, cm1) m: 3176 (N–H), 2924 (C–H),1698 (C,N), 1463 (C,C), 1376 (C–N), 1151 (C–O), 722(C–Cl), 521 (C–Br). ^{1}H NMR

(DMSO-d6, 400 MHz)d: 10.1(s, 1H, NH), 8.55 (s, 1H, Pyrimidine-H), 7.69 (d, 2H, Ar-H), 7.61 (d, 2H, Ar-H), 6.64 (d, 1H, Ar-H), 6.46 (d, 1H, Ar-H), 6.41 (s, 1H, Ar-H), 3.81 (s, 3H, OCH3). MS (ESI)m/z: 529.0. Anal. calcd. for C20H19BrClN3O3S2(in %): C-45.42, H-3.62, N-7.95. Found C-45.62, H-3.72, N-8.12.

2.2. Single crystal X-ray crystallography

Single crystal X-ray diffraction is employed to study the crystal structure of the title compound, and their diffraction data were collected by using Bruker kappa APEX II single crystal X-ray diffractometer contains graphite monochromatedMo$K\alpha$ radiation with a wavelength λ= 0.71073 Å at 293K. Multi-scan absorption corrections were applied using the SADABS program. The structure was solved using the directed methods and refined by the full matrix least-squares technique using SHELXS-97 [16] and SHELXL-2018/3 [19] respectively. The non-hydrogen atoms were refined with anisotropic displacement parameters. All hydrogen atoms were included in their calculated positions, assigned fixed isotropic thermal parameters, and constrained to ride on their parent atoms. The standard geometrical calculations were done using the program PLATON [20] and the thermal ellipsoidal plot was generated using the software Mercury4.0 [21].

2.3. Computational methods

The structure of the title compound was optimized in the gas phase using the Gaussian 09 program [22] with the B3LYP method at the 6-311++G(d,p) for all atoms. Geometry optimizations were tested by frequency analysis to ensure that they were at the minima of potential energy surface (PES). The results showed that there were no imaginary frequencies. The highest occupied molecular orbital and lowest unoccupied molecular orbital (HOMO-LUMO), their energy gap, and global reactive parameters were calculated using the Koopman's approximation [23]. 3D molecular orbitals were visualized in Gaussview 06 [24]. The molecular electrostatic potential (MEP), was carried out to determine the plausible reactive sites and charge distribution of the title molecule. The quantum theory of atoms in molecules (QTAIM) and reduced density gradient (RDG) analyses were done to unravel the electron density values the bond critical points (BCPs) and to explore the weak interactions present in the molecule. The desired calculations for MEP, QTAIM, and RDG were done using Multiwfn 3.7 [25] package and visualized in the software Visual Molecular Dynamics [26] software. Further, natural bond order calculations were performed to know the hyperconjugative interactions which are involved to stabilize the molecular structure. In addition, the above said method is used to compute certain thermodynamic properties.
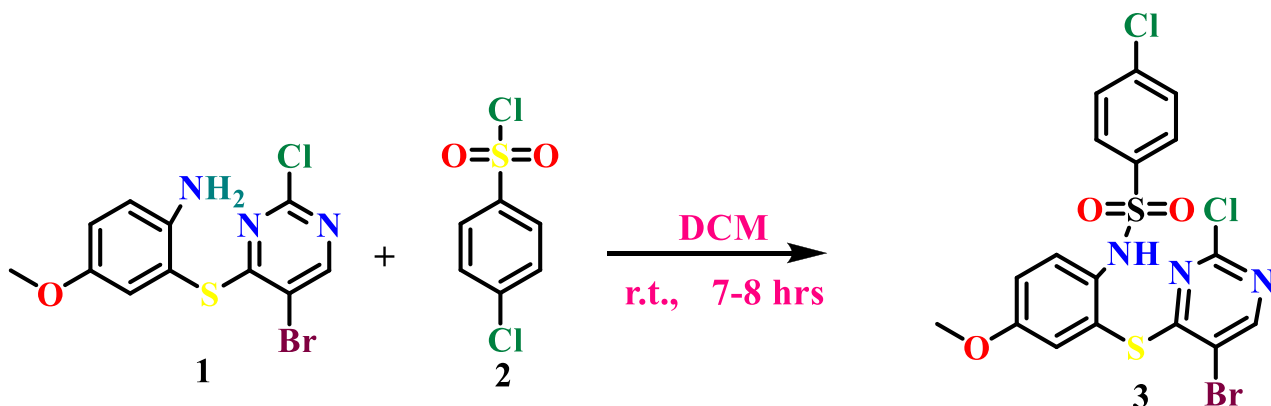
Scheme 1. Synthetic route for title compound.

Table 1
Crystal data and structure refinement details of the title compound.

Parameter	Value
Empirical formula	$C_{17}H_{12}BrCl_2N_3O_3S_2$
Formula weight	521.22
Temperature	300 K
Wavelength	0.71073 Å
θ range	1.89° - 26.00°
Crystal system	Triclinic
Space group	*P* -1
Cell parameters	a = 12.4079(14) Å
	b = 13.2405(15) Å
	c = 13.7416(15) Å
	α = 69.616(3)
	β = 81.345(4)
	γ = 77.404(4)°
Volume	2058.4(4) Å³
Z	4
Density (calculated)	1.682 Mg m⁻³
Absorption coefficient	2.483 mm⁻¹
F_{000}	1040
Crystal size	0.20 mm ✗ 0.15 mm ✗ 0.10 mm
Index ranges	−15 ≤ h ≤ 15
	−16 ≤ k ≤ 16
	−16 ≤ l ≤ 16
Reflections collected	43599
Independent reflections	8013 [R_{int} = 0.0543]
Absorption correction	Multi-scan
Refinement method	Full matrix least-squares on F^2
Data/restraints/parameters	8013/0/590
Goodness-of-fit	1.030
Final [$I > 2\sigma(I)$]	R_1=0.0360, wR_2=0.0846
R indices (all data)	R_1=0.0562, wR_2=0.0915
Largest diff. peak and hole	0.402 and – 0.505 e Å⁻³

3. Results and discussions

3.1. X-ray structure analysis

N-[2-(5-bromo-2-chloro-pyrimidin-4-yl)thio)-4-methoxy-phenyl]-4-chlorobenzenesulfonamide compound is crystallized in triclinic *P*-1space group confirmed by the single crystal X-ray structural analysis. The crystal data and structure refinement details are summarized in the Table 1.

The analysis clearly revealed the dimeric existence of the title compound is shown in the *ORTEP* (Fig. 1a). The dimer molecules D1 and D2 are highly non planar and their molecular orientations are distinct to each other. In D1, chlorobenzene and chloro-bromo substituted pyrimidinyl rings are twisted oppositely with respect to methoxyphenyl moiety with the ring centroids and plane distance of 3.47 Å and 2.62 Å respectively, while in D2 these rings are oriented face to face with the ring centroids distance of 3.552 Å leading to the weak intramolecular Pi-stacking interactions (Fig. 1b and c). Distortion of sulfonamide moiety with respect to methoxyphenyl and chlorobenzene rings is measured as 63.29° of torsional angle (C17A-S2A-N3A-C5A) in dimer molecule D1, whereas the same is measured for dimer molecule D2 as 80.18° of torsional angle (C12B-S2B-N3B-C5B), is shown in supplementary figure S1.

Crystal packing of the title compound is characterized by several intra and intermolecular hydrogen bond interactions, intermolecular halogen (chloro...chloro, chloro...bromo and bromo...bromo) contacts, intra and intermolecular Cg-Cg stacking, intermolecular Y-X...Cg(Pi-Ring; Table 2) interactions and short non-hydrogen inter-molecular contacts. Oxygen atoms of sulfonamide moieties in D1 and D2 acts as hydrogen acceptors leads to the formation of intermolecular hydrogen bond interactions with the the CH and NH groups. Sulfonamide oxygen O3A in D1 played a major role in connecting adjacent D1 molecules with the

several intermolecular interactions such as N1A...O3A, N2A...O3A, C14A...O3A, C15A...O3A non-hydrogen short interactions and N2A-H21A...O3A hydrogen bond interaction which lead to formation of $R_2^2(8)$ ring motif (Fig. 2a). All the interactions exhibited by D1 sulfonamide O3A atom, are contributed to one-dimensional inter-molecular clusters along crystallographic c-axis (Fig. 2b) and these clusters are interconnects through chloro-bromo halogen interactions (Fig. 2c) lead to form layers of clusters along ab-pane where these layers are further interconnected via Cl2A...C3A short interactions (supplementary figure S2).

The dimer molecule D2 also exhibits multiple intermolecular interactions with the adjacent molecules. All three oxygen atoms of D2 molecules involved in the hydrogen bonding by acting as a hydrogen acceptor from the methoxyphenyl and chlorobenzene rings (Table 2). C7B-H4B...O1B, C3B-H5...O3B and C13B-H2B...O2B type of hydrogen bond interactions exhibited by the adjacent D2 molecules construct the $R_2^2(8)$, $R_2^2(14)$ and $R_2^2(10)$ synthons respectively leading the parallel molecular chains on the crystallographic ac-plane (Fig. 3a). These three C-H...O hydrogen bonds connects eight neighboring D2 molecules and form $R_6^6(32)$ supramolecular ring synthon along b-axis (Fig. 3b). Apart from the hydrogen bond interactions, halogen interaction between adjacent D1 and D2 molecules also played a major role in crystal packing of title compound. Chloro...bromo (Br1A...Cl2A: 3.553 Å) interactions between D1 molecules, chloro...chloro (Cl1A...Cl2B: 3.401 Å) between D1 and D2 molecules and bromo...bromo (Br2A...Br2A: 3.455 Å) interactions between D2 molecules, greatly characterized the crystal packing of title compound by L shaped molecular arrangement on bc-plane (Fig. 3c). Further C14A-Cl2A...Cg4 [Cl2A...Cg4: 3.974(2) Å, C14A...Cg4: 4.066(4) Å, C14A-Cl2A...Cg4: 106.46(5)° and symmetry code: x,y,-1+z] and S1A-O3A...Cg1 [O3A...Cg1: 2.882(2) Å, S1A...Cg1: 3.853(3) Å, S1A-O3A...Cg1: 122.98(13)° and symmetry code: -x,1-y,1-z where Cg1 and Cg4 are the centroid of the chloro-bromo pyrimidinyl rings of D1 and D2 molecules respectively (Fig. 3d). Crystal packing of the title compound is also characterized by inter and intramolecular $\pi...\pi$ interactions, where these contacts exceedingly contribute to the crystal structure stability [27,28]. Intra $\pi...\pi$ interactions between chloro-bromo pyrimidinyl ring and chlorobenzene is explored in D2 with the centroid-centroid distance of 3.552 Å, where as inter $\pi...\pi$ interactions occurred between Cg1 of D1 and Cg5 of D2 (Cg5: centroid of chlorobenzene ring in D2) with a distance of 3.534 Å (figure 3e).

3.2. Hirshfeld Surface (HS) analysis

The HS is defined as the space occupied by the molecule in a crystal based on electron distribution calculated as the sum of the spherical atom electron densities. HS analysis combined with the fingerprint plot (FP) is a effective tool to investigate the intermolecular interactions present within a crystal structure of a molecule[28]. The HS and FP's for the title molecule were generated using CrystalExplorer 17.5 [29] software.

The d_{norm} surface for the molecule in the asymmetric unit of the crystal structure has been shown in Fig. 1(a) (front view) & 1(a') (rear view). The bright red spots appeared in the d_{norm} surfaces suggest that the existence of intermolecular hydrogen bond contacts. The deep red spot on HS appeared in the Fig. 4(a) indicates the C3B-H5...O3B and N3B-H15...N2A interactions in the crystal. This C3B-H5...O3B interaction is responsible for forming $R_2^2(8)$ supramolecular synthons. Similarly, the intense red spot on the HS in the Fig. 4(a') displayed that existence of C15A-H22...N2B and N3A-H21...O3A interactions present in the crystal and 4 (a'') showed the existence of halogen...halogen interactions in the title molecule. From the Fig. 4b, it is evident that the molecules are related to each other by π-π stacking interactions, as can be observed from the inspection of the adjacent red and blue patches
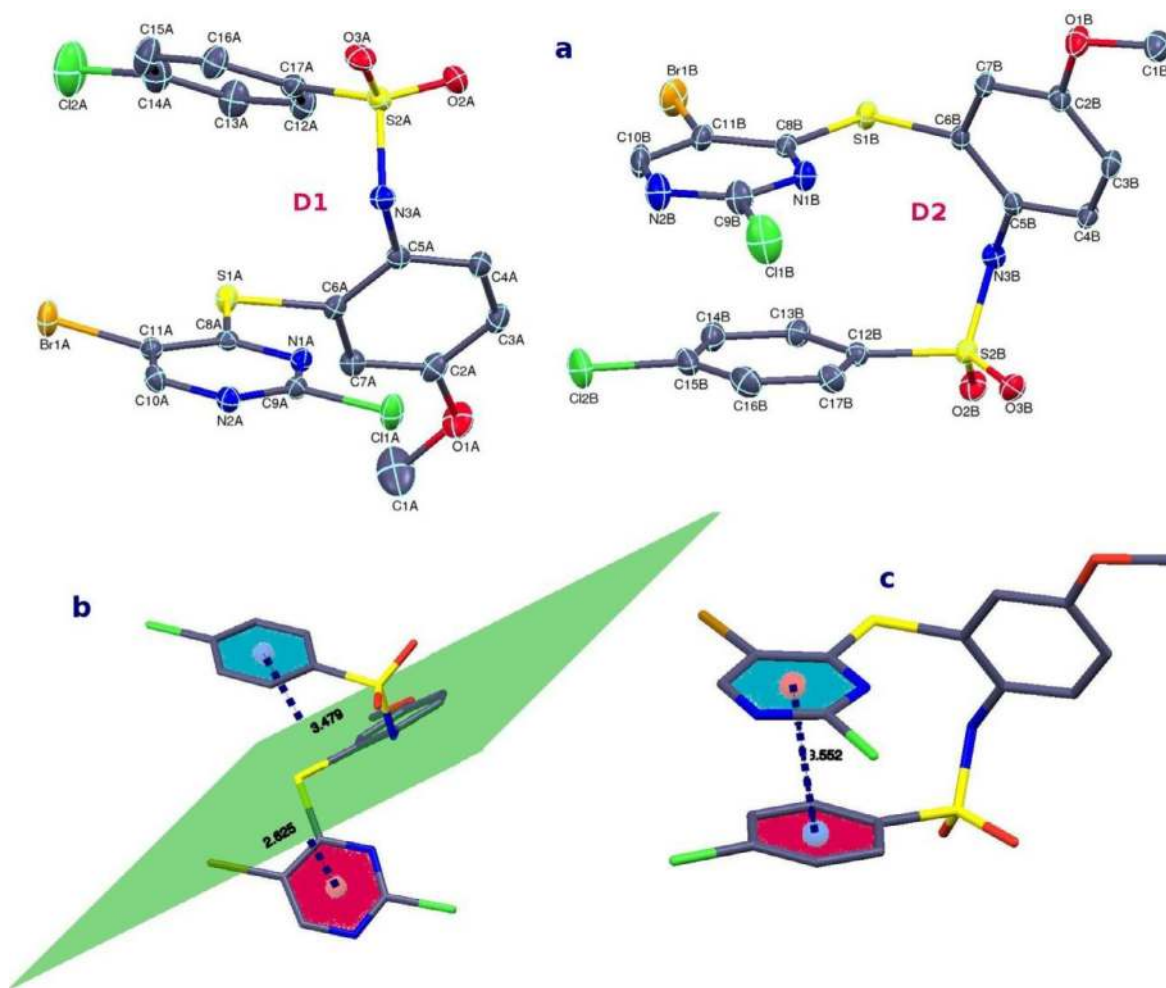
Fig. 1. (a) *ORTEP* with atom numbering scheme where thermal ellipsoids drawn at 30% probability, (b and c) planarity comparison of the dimer molecules D1 and D2, where distinct orientation is observed between methoxyphenyl and chlorobenzene rings of D1 and D2.

Table 2
Intra and intermolecular hydrogen bond geometry of the title molecule.

| D-H...A	D-H (Å)	H...A (Å)	D...A (Å)	D-H...A (Å)
N3B-H15...N2A[i]	0.75 (3)	2.29 (3)	3.033 (3)	174 (3)
N3A-H21...S1A[a]	0.83 (3)	2.87 (3)	3.131 (3)	100.6 (19)
N3A-H21...N1A[a]	0.83 (3)	2.60 (3)	3.119 (3)	122 (2)
N3A-H21...O3A[ii]	0.83 (3)	2.26 (3)	3.055 (3)	162 (2)
C17B-H1...O3B[a]	0.95 (4)	2.53 (4)	2.915 (4)	104 (3)
C3B-H5...O3B[iii]	0.92 (3)	2.50 (3)	3.384 (3)	161 (2)
C16A-H13...O3A[a]	0.91 (4)	2.54 (4)	2.943 (4)	108 (3)
C15A-H22...N2B[ii]	1.00 (4)	2.46 (4)	3.387 (5)	154 (3)
Symmetry code **i**: x, 1+y, z; **ii**: -x, 1-y, 1-z; **iii**: 1-x, 2-y, 2-z			a-intramolecular interactions	

on the shape index surface. Also, π-π interactions are evident on the HS as a large flat region across the molecule, which is most clearly visible on the curvedness surfaces (Fig. 4c). The electrostatic potential map (Fig. 4d) highlights the electropositive (blue) and electronegative (red) regions on the surface. The molecule shows red (hydrogen bond acceptors) colored regions around the oxygen atom (O1, O2, and O3), indicating the electronegative spots and the blue (hydrogen bond donors) colored region near the nitrogen atom (N3) indicates the electropositive spot. The voids present in the crystal packing are a good indicator to find out how closely the molecules are arranged with one another. The less percentage

of voids signifies stronger crystal packing. These voids are calculated based on the sum of spherical atomic electron densities at the appropriate nuclear positions [30]. The crystal void calculation reveal that the void volume is of the order of 313.98 Å³ of the title molecule. The surface area is found to be 855.91 Å². Fig. 4e shows the voids in the crystal structure.

The 2D fingerprint plots are investigated to get the individual contribution of H-H (24.5%), O-H (19.8%), Cl-H (9.1%), and Br-H (8.6%) intermolecular interactions which have comprised total HS (Fig. 5). The pairs of spikes in the Cl-H and Br-H FP plots correspond to Cl...H and Br...H contacts, respectively and reveals the oc-
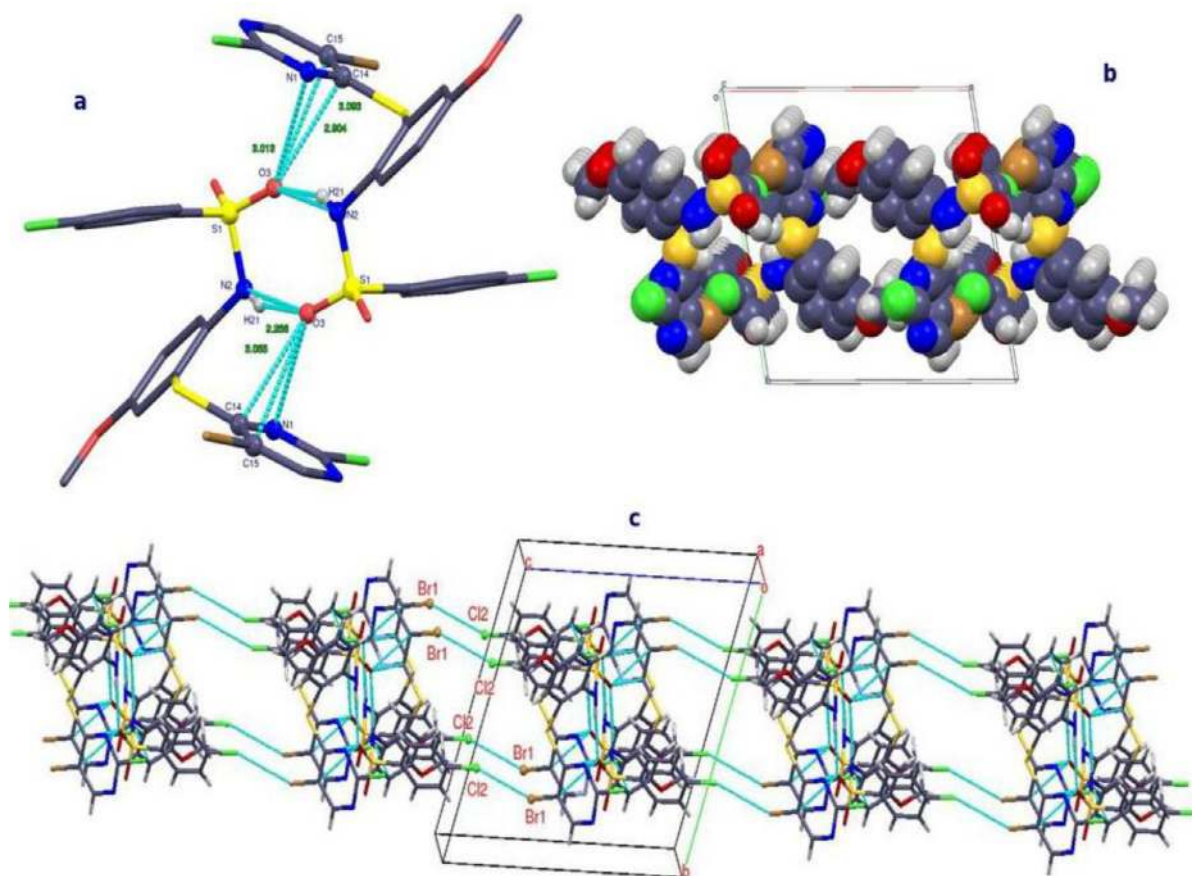
Fig. 2. N-H...O intermolecular interactions between adjacent D1 molecules lead to formation of supramolecular rings (a) and 1D intermolecular clusters along crystallographic c-axis (b), and these clusters interconnected by chloro-bromo halogen interactions (c).
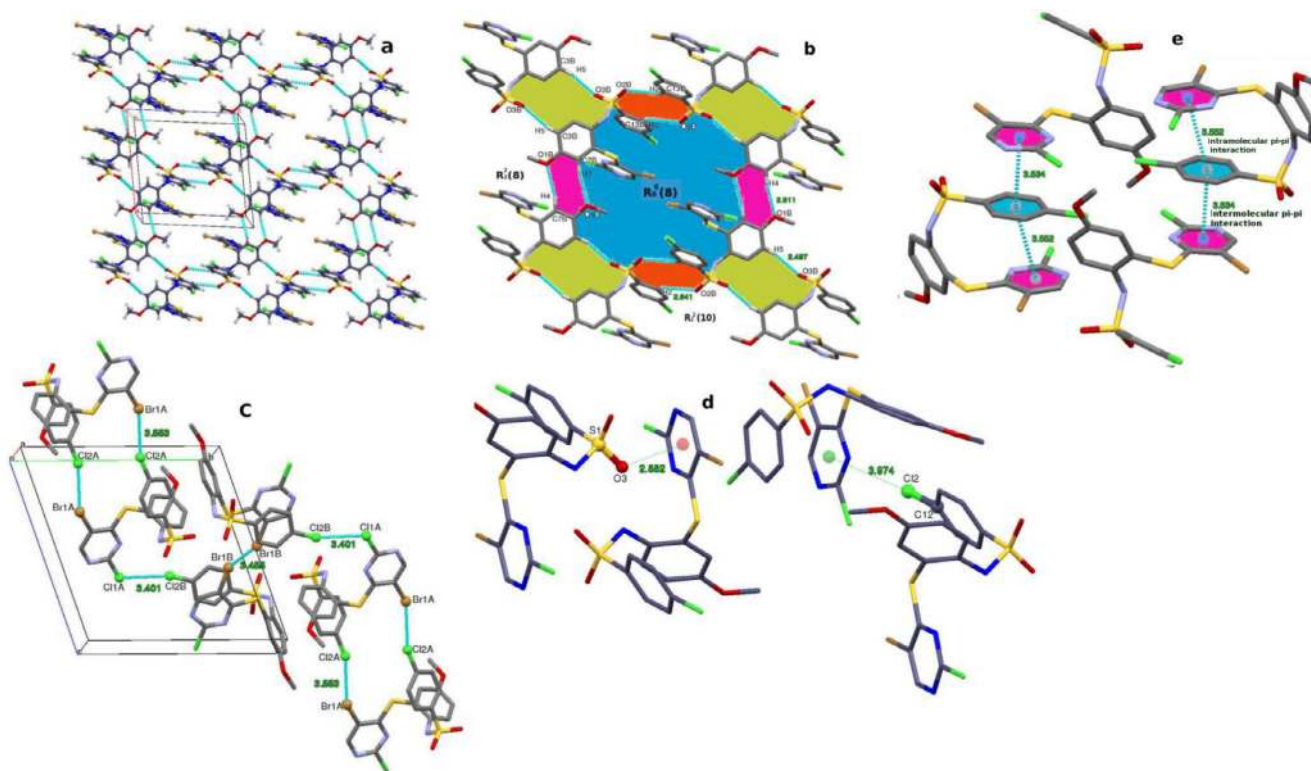

Fig. 3. Multiple intermolecular hydrogen bond interactions existed in dimeric D2 molecule contributed to the formation of several supramolecular ring motifs along b-axis (a and b), distinct halogen interactions (c), intermolecular C-Cl...Cg and S-O...Cg interactions (d) and π...π interactions (e) between adjacent D1 and D2 molecules.
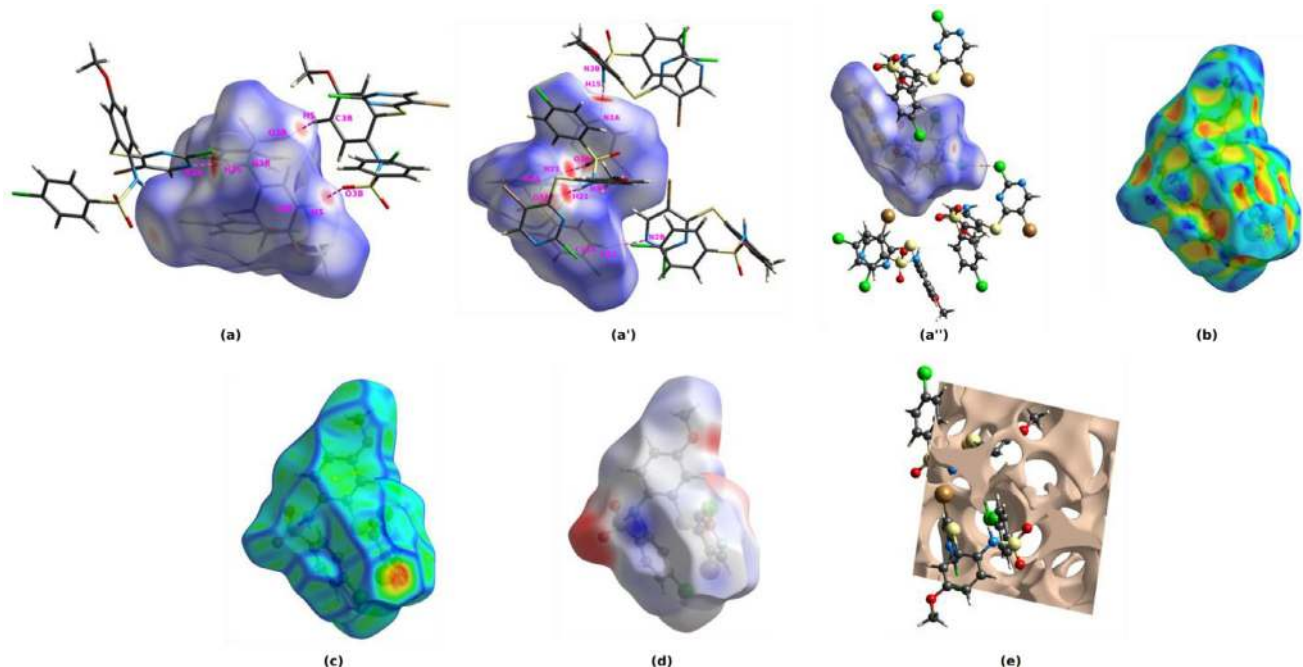
Fig. 4. (a) d_{norm} surface (front view), (a') d_{norm} surface (rear view), (a'') d_{norm} surface showing halogen...halogen (Br...Br and Cl...Cl) interactions, (b) shape index, (c) curvedness, (d) electrostatic potential and (e) voids showed in the crystal structure of the title molecule.
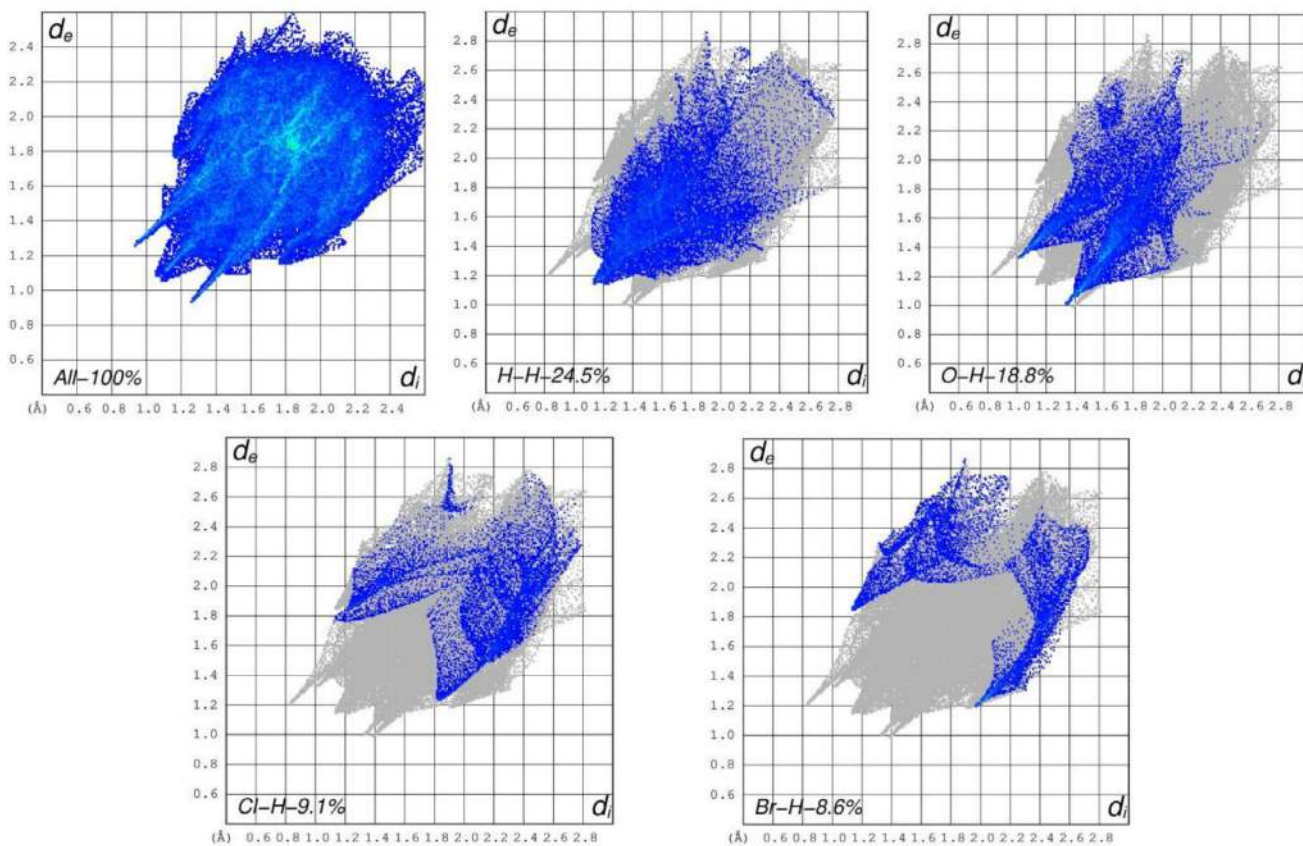
Fig. 5. 2D FP's of the title molecule.
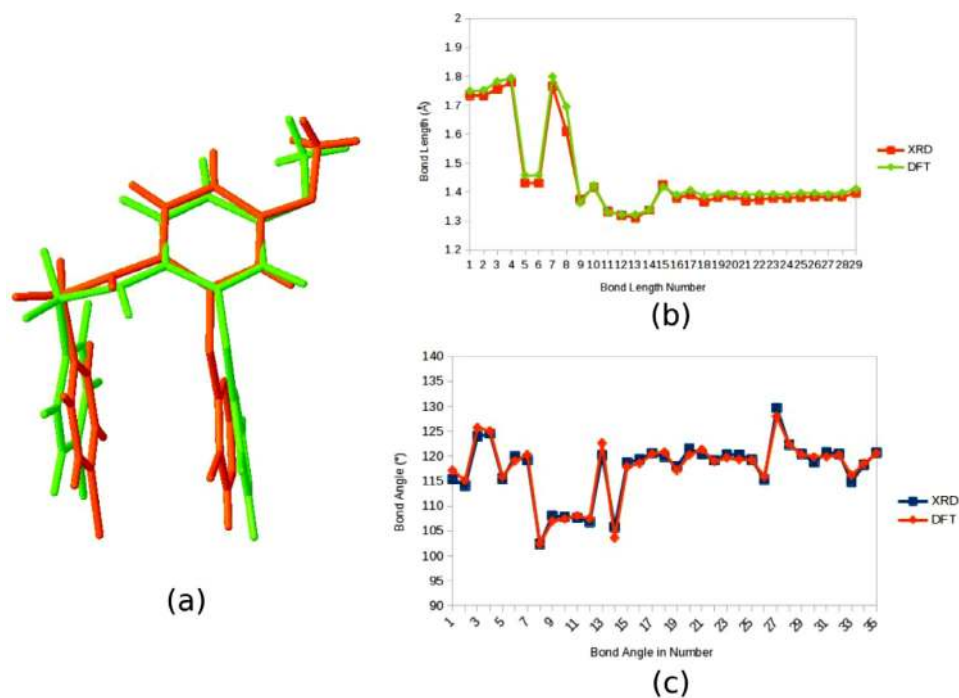
Fig. 6. (a) Overlay diagram of the title molecule obtained by XRD (green) and DFT (orange), (b) and (c) graph of bond length and bond angle vs bond length number and bond angle number.

currence of weak Cl...H and Br...H interactions, which are visible in the Hirshfeld surfaces (Fig. 4 a''). The blue -green region on the FPS indicate the π-π interactions.

3.3. Molecular geometry

The optimized molecular geometry of the title molecule was performed using DFT calculations with 6-311++G(d,p) basis set [31]. The geometrical parameters have been observed from an optimized molecular structure and summarized in table S1, S2, and S3. The theoretically calculated bond lengths, bond angles, and torsion angles were matched with the XRD data. In this study, theoretic calculations has been carried out in the gas phase and experimental part has been done in the solid phase. Hence the comparison of these results show that the majority of the theoretical parameters are slightly greater than the experimental results. The molecular structure of the asymmetric unit of the title molecule, obtained from XRD and DFT methods have been overlaid and its shown in the Fig. 6 and RMSD value found to be 0.876 Å (without inversion).

3.4. Frontier molecular orbitals (FMOs) and global reactive parameters

The DFT calculations furnishes some important information regarding the reactivity and site selectivity of the molecular framework. The energy of the HOMO is concerned to the ionization potential, while the energy of LUMO is related to electron affinity. The energy gap between the HOMO and LUMO characterizes the molecular chemical stability. The 3D molecular orbitals are illustrated in Fig. 7. Red and green color distribution indicate positive and negative phase in molecular orbital wave function respectively. The HOMO-LUMO energy gap of the title molecule is found to be 4.11 eV which is slightly less compared to the same derivative of the reported compound (4.239 eV). This is due to the fact that functional group leads to the change in the property of the molecule [32]. A molecule having a large HOMO-LUMO gaps is a hard molecule and with small HOMO-LUMO gap a soft molecule
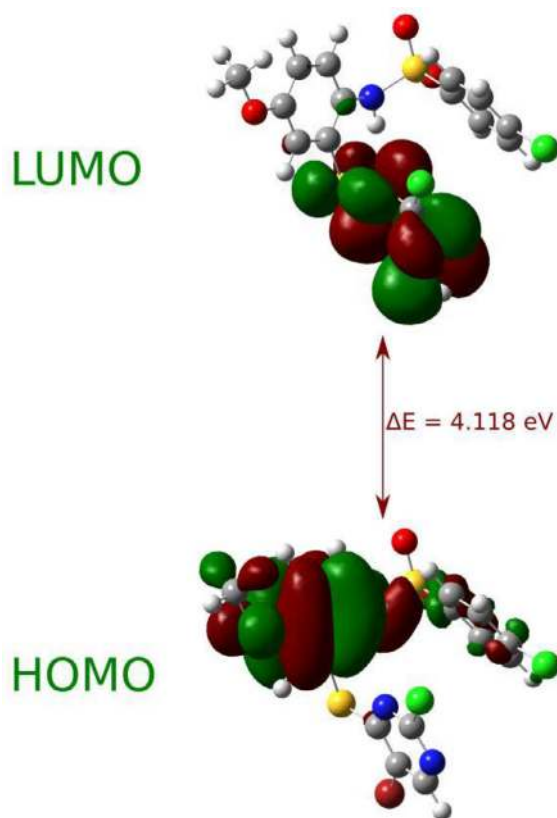
Fig. 7. 3D HOMO-LUMO orbital diagram of the title molecule.

being more reactive. Soft systems are large and highly polarizable while hard systems are relatively small and much less polarizable. The electron density of HOMO and LUMO in the title compound is concentrated on the 4-methoxyphenyl group of the molecule and 5-bromo-2-chloro-4-pyrimidinyl group respectively.

Table 3
Energies of HOMO-LUMO and global reactivity parameters of the title molecule.

Parameters	Value
E_{HOMO}	-6.363 (eV)
E_{LUMO}	-2.245 (eV)
Energy gap (ΔE)	4.118 (eV)
Ionization energy (I)	6.363 (eV)
Electron affinity (A)	2.245 (eV)
Electronegativity (χ)	4.304 (eV)
Chemical potential (μ)	-4.304 (eV)
Global hardness (η)	2.059 (eV)
Global softness (s)	0.486 (1/eV)
Electrophilicity index (ω)	4.498 (eV)

The magnitude of global reactivity parameters are summarized in the Table 3 were calculated with the help of energies of HOMO-LUMO. The global electrophilicity index (ω), global hardness (η), chemical potential (μ), and global softness (s) are known as global reactivity parameters [33,34]. The chemical potential is the escaping tendency of electrons from a stable system, the negative chemical potential signifies molecule to be stable that does not decompose spontaneously into its elements. The chemical potential has -4.304 eV value for the title molecule; hence it is more stable in nature. The hardness indicates the resistance toward the deformation of electron cloud of chemical system under small perturbations encountered during chemical process. Lesser the value of chemical hardness 2.059 eV, is more reactive in nature. The local hardness furnishes the information about the intermolecular reactivity, whereas the global hardness about the stability of the molecule. Electrophilicity is concerned to ability of an electrophile to acquire additional electronic charge and the resistance to exchange electron transfer and stability.

3.5. Molecular electrostatic potential (MEP) analysis

MEP map is a three-dimensional diagram which can be used to visualize the reactive sites and charge distribution of the molecules. It exemplifies the plausible sites for electrophilic and nucleophillic attacks and is useful in biological recognition processes and hydrogen bonding interactions. Visual understanding of the polarity of the molecule is also achieved with this calculation. The color scale represents the electrostatic potential region on the surface of the molecule; red represents areas of most electronegative electrostatic potential; blue indicates the region of most positive electrostatic potential and green represents areas of zero potential. The electrostatic potential value ascends in the order red < green < blue [35,36].

The MEP map of the sulfonamide derivatives is shown in Fig. 8. From the figure, one can observe that the negative electrostatic potential corresponds to an attraction of a proton by the cluster of electron density in the molecule (shades of red color) and the positive electrostatic potential corresponds to the repulsion of a proton by the nuclei (shades of blue). The color code of this MEP map ranges from -35 kcal/mol to +31 kcal/mol. Fig. 5 reveals that negative regions are localized over the O atom which is the most reactive site for an electrophilic attack, whereas most positive regions are around the H atoms which are most reactive sites for a nucleophilic attack. As expected, the heaviest halogen atom (Br) atom presents the largest and more intense σ-hole to establish halogen bonding interactions. In contrast, the chlorine atom shows a very small and positive MEP value. The MEP map of electrostatic potential confirms the different negative and positive potential sites of the molecule in accordance with the total electron density surface map.
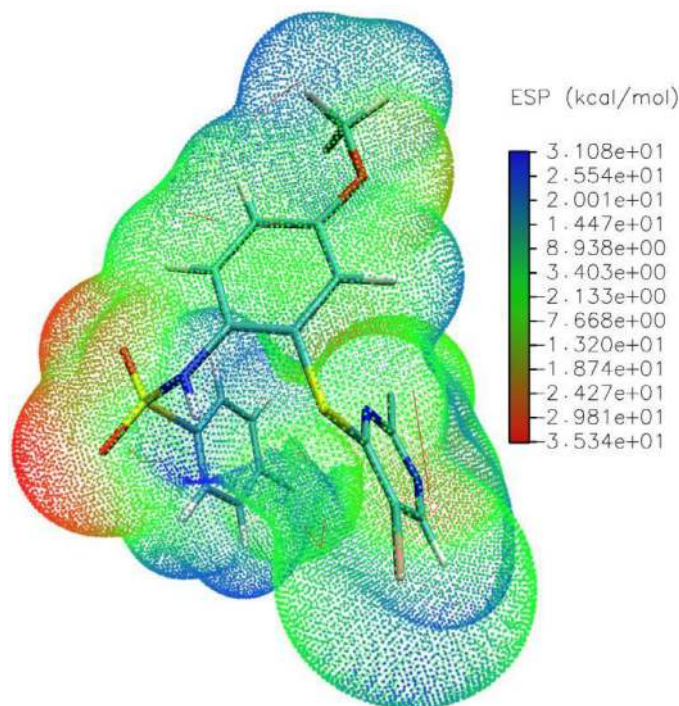
Fig. 8. MEP map of the title molecule.

3.6. Natural bond orbital (NBO) analysis

The natural bond orbital is an efficient method for studying interactions among various bonds with a convenient basis for investigating charge transfer in a molecular system. The most important advantage of the NBO analysis is the information obtained about the interactions in both filled and the virtual orbital which supplement the analysis of both the intra and intermolecular interactions. The strength of the interactions between donors and acceptors, or the donating tendency among donors and acceptors and hence the degree of conjugation of the system is measured by the value of energy of the hyperconjugative interactions $E^{(2)}$.

In order to examine the donor-acceptors interactions, the second order Fock matrix was done in NBO analysis [37]. For each donor (I) and acceptor (j), the stabilization energy $E^{(2)}$ associated with the delocalization i→j is estimated as:

$$E^{(2)} = \Delta E_y = q_i \frac{F^{(2)}(ij)}{\varepsilon_j - \varepsilon_i}$$

where q_i is the donor orbital occupancy. ε_j and ε_i are diagonal elements and $F(i,j)$ is the off diagonal NBO Fock matrix element. The larger the $E^{(2)}$ value the greater will be the extent of conjugation of the molecular system due to the more donating tendency from donor-acceptors. Hence Table 4 gives the interaction between the electron donors and acceptors present in the molecule.

The conjugation of the molecule σ(O2-S2)→σ*(O3-S2) results in the more stabilization of the structure. The electron donation from the loan pair LP(2) to the antibonding acceptor (π*) is related to the resonance in the molecule and contributes towards the stabilization energy of the molecular structure. The delocalization of the electron density between the occupied and unoccupied NBOs results in the intramolecular charge transfer (ICT) corresponds to the stabilization of the molecular system. For example, π(C7-N2) → π*(C12-C14), π(C9-C10) → π*(C7-N2), and π(C8-N1) → π*(C9-C10) with stabilization energies 33.01, 29.12, and 29.03 respectively.

Table 4

Second-order perturbation theory analysis of Fock matrix in NBO basis corresponding to the intramolecular bonds of the title molecule.

Donor (i)	Occupancy	Acceptor (j)	Occupancy	E(2)	E(i)-E(j)	F(i,j)
$\sigma_{(O2-S2)}$	1.9856	$\sigma^{*}_{(O3-S2)}$	0.14641	813.21	0.36	0.28
$\pi^{*}_{(C1-C2)}$	0.3772	$\pi^{*}_{(C16-C17)}$	0.3022	225.24	0.01	0.08
$\pi^{*}_{(C8-N1)}$	0.4209	$\pi^{*}_{(C9-C10)}$	0.3199	197.12	0.02	0.08
$\pi^{*}_{(C6-C11)}$	0.4460	$\pi^{*}_{(C12-C14)}$	0.3914	195.26	0.02	0.09
$\pi^{*}_{(C7-N2)}$	0.4537	$\pi^{*}_{(C9-C10)}$	0.3199	135.73	0.02	0.08
$\sigma_{(C5-C6)}$	1.8558	$\pi^{*}_{(C5-C15)}$	1.5344	43.5	0.71	0.17
$\sigma_{(C5-C15)}$	1.9234	$\sigma^{*}_{(C5-C6)}$	0.0869	41.83	0.83	0.19
$\sigma_{(C13-H40)}$	1.9909	$\sigma^{*}_{(O2-S2)}$	0.1393	39.16	3.61	0.35
$\pi_{(C7-N2)}$	1.7163	$\pi^{*}_{(C8-N1)}$	0.4209	33.01	0.31	0.093
$\pi_{(C5-C15)}$	1.5344	$\pi^{*}_{(C12-C14)}$	0.3914	29.43	0.21	0.07
LP(2)$_{(O3)}$	1.8424	$\pi^{*}_{(C12-C14)}$	0.3914	29.42	0.34	0.1
$\pi_{(C9-C10)}$	1.6737	$\pi^{*}_{(C7-N2)}$	0.4537	29.12	0.27	0.08
$\pi_{(C8-N1)}$	1.7181	$\pi^{*}_{(C9-C10)}$	0.3199	29.03	0.32	0.09
LP(2)$_{(S1)}$	1.7938	$\pi^{*}_{(C7-N2)}$	0.4537	26.89	0.22	0.07
$\sigma_{(C5-C15)}$	1.5344	$\sigma^{*}_{(C5-C6)}$	0.0869	41.83	0.83	0.19

Table 5

Topological parameters computed at BCP (3, -1) for the title molecule. All the parameters are in a.u. except for E_{HB} (kcal/mol).

| Interactions	BCPs	$\rho(r)$	$\nabla^2\rho(r)$	G(r)	V(r)	$-\frac{G(r)}{|V(r)|}$	E_{HB}
Cl...Br	398	0.00777	0.0299	0.00595	-0.00442	1.346	1.386
Cl...Cl	349	0.00185	0.00622	0.00116	-0.000765	1.516	0.4800
C-H...Br	281	0.00999	0.03533	0.00738	-0.00592	1.246	3.714
C-H...Br	189	0.01048	0.03676	0.00769	-0.00620	1.240	3.890
C-H...Cl	369	0.00212	0.00822	0.00144	-0.00083	1.734	0.520
C...Br	207	0.00448	0.0136	0.002733	-0.002055	1.333	3.172
C...Cl	298	0.00250	0.00787	0.00156	-0.00116	1.344	0.727

3.7. QTAIM and NCI analysis

According to Bader's, quantum theory of atoms in molecules (QTAIM), the electron density $\rho(r)$ is the more accurate descriptor of electronic structure of the molecules. The topological analysis of $\rho(r)$ and its Laplacian $\nabla^2\rho(r)$ helps to determine whether an H-bond is present between the H-bond donor group and an acceptor group. The magnitude of $\nabla^2\rho(r)$ at bond critical points (BCP) signifies the degree of electron density concentration or depletion and this can be used to distinguish between shared shell and closed shell bonding interactions. Also, the value of $\rho(r)$ can be related to hydrogen bond energy E_{HB} [38]. Along with $\rho(r)$ and $\nabla^2\rho(r)$, kinetic energy density G(r), potential energy density V(r), $E_{HB}=V(r)/2$ and $|V(r)|/G(r)$ are also the effective parameters to characterize the H-bonding. The topological parameters are computed at BCP (3, -1) and the results are summarized in Table 5. The V(r) value is correlated with H-bond energy E_{HB} [39]. The ratio, $|G(r)|/V(r)$, has a greater than 2 for covalent bonds. If the ratio between 1 and 2 is for mixed character interactions and the value lower than 1 for the ionic, H-bond and van der Waals interactions. It is clear from Table 5 that all the weak halogen interactions within in the title

molecule are noncovalent or closed shell nature, since their $\rho(r)$ values are less than 0.10 a.u. Moreover, the corresponding $\nabla^2\rho(r)$ are all positive and falls within the range 0.008-0.03 a.u. The weak halogen interactions studied here are characteristics of noncovalent nature because the ratio $-\frac{G(r)}{|V(r)|} > 1$.

Noncovalent interactions (NCI) method developed by Johnson *et al* evaluate the molecular bonding and nonbonding interaction regions by the reduced density gradient and is defined by [40,41].

$$RDG(r) = \frac{\Delta\rho(r)}{2\left(3\pi^2\right)^{1/3}\rho(r)^{4/3}}$$

The isosurface exemplify the different kinds of NCI directly in real space via color codes. It enables one to distinguish the attractive or repulsive nature of the interactions and to decide their relative strength on a qualitative but visual basis. Blue, green and red color indicate the strong attraction (H-bonding), very weak interactions (van der Waals interactions), and strong repulsion (steric clashes) respectively. The NCI isosurface for the title molecule is shown in Fig. 9 (b).The green color isosurface revealed that the presence of weak interactions (van der Waals interactions) and the
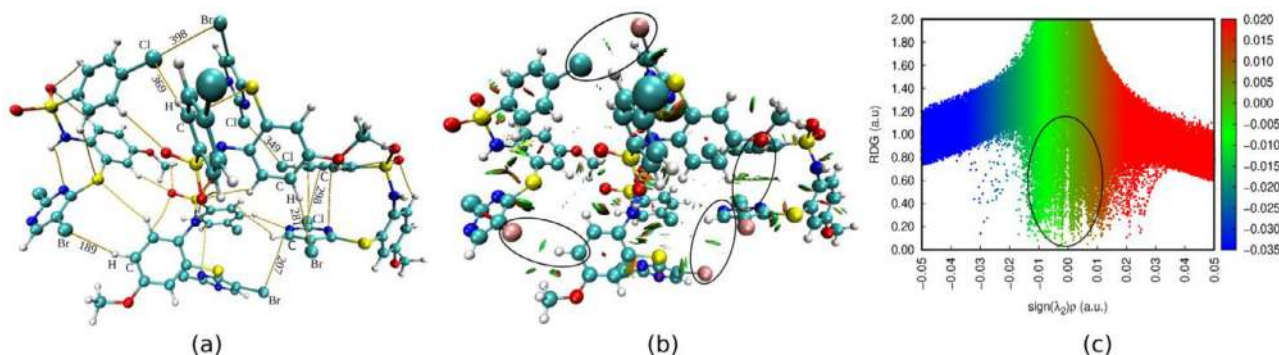
Fig. 9. (a) molecule with intermolecular interaction from QTAIM analysis, (b) Non-covalent interactions (NCI) isosurfaces of electron density for the title molecule, and (c) 2D scattered map of RDG vs sign(λ_2)$\rho(r)$.

results are consistent with the E_{HB} obtained by the QTAIM analysis. The red colored isosurface indicates the steric interactions involved in the molecule. Also, the green colored peaks appeared in the low density region in the 2D scatter map of RDG vs sign(λ_2)ρ(r) unravels the weak interactions of the title molecule. Similarly, the red colored peaks in the large density region indicates the steric clashes involved in the molecule. The absence of blue colored isosurface in the NCI isosurface and blue peaks in the 2D scattered map indicates that there is no strong hydrogen bond interaction in the molecule. The ellipsoidal mark in the Fig. 9 (b) indicates the existence of weak halogen bond interactions in the title molecule.

4. Conclusion

In the present study, A novel pyridine containing sulfonamide derivative was synthesized and its structure is affirmed by the single crystal X-ray diffraction study. Authors have explored the orientational features of the title compound and the role of various interactions like noncovalent interaction, halogen interactions in crystal packing. The structural analysis revealed that the title molecule exists in dimer, which connects via halogen interactions. The analysis of supramolecular self assembly of the molecular shows that H-bonding interactions are involved in the crystal packing. Hirshfeld surface analysis revealed the H-bonding and Ha...Ha bonding intermolecular interactions which are mainly responsible for the crystal packing. Also, the title compound has been subjected to theoretical studies using DFT calculations. The structural overlay signifies the good correlation between the results of XRD and DFT studies. The HOMO-LUMO energy gap was found to be 4.118 eV, which shows that the title molecule has good stability and high chemical hardness. The MEP map of the title compound indicates the reactive sites present in the molecule. The natural bonding orbital analysis shows that the $\sigma_{(O2-S2)} \rightarrow \sigma^*_{(O3-S2)}$ interaction having highest stabilization energy 813.21 kJ/mol. The QTAIM and NCI analysis further validates the existence of halogen bonding interactions in the title compound, and the topological properties of halogen bond critical points (BCPs), such as the electron density ρ(r) and its Laplacian $\nabla^2\rho$(r), are shown to correlate well with the interaction energy. The electron densities at the BCPs can be considered as a good description of the strength of halogen bonding. In view of these conclusions reached, authors can expect that the nature and magnitude of halogen bonding interactions described in this work would be very useful in the design and synthesis of new materials and effective drugs involving aromatic halogen compounds.

Credit author statement

CSK, PM and LM. - Synthesis, Manuscript work design and writing.

MKH and NKL – Single crystal XRD and Manuscript writing and corrections.

TNL and MAS – DFT, HAS and Manuscript writing.

SS, RRJ and KM - Contributed for language polishing manuscript corrections.

Declaration of Competing Interest

The authors declare that they have no known competing financial interests or personal relationships that could have appeared to influence the work reported in this paper.

Acknowledgment

Supplementary materials

Supplementary material associated with this article can be found, in the online version, at doi:10.1016/j.molstruc.2022.133476.

References

[1] K. Liu, Y. Kang, Z. Wang, X. Zhang, 25th anniversary article: reversible and adaptive functional supramolecular materials:"Noncovalent interaction" matters, Adv. Mater. 25 (39) (2013) 5530–5548.

[2] T.C. Raveesha, M.K. Hema, K.J. Pampa, P.G. Chandrashekara, K. Mantelingu, T. Demappa, N.K. Lokanath, Analysis of supramolecular self-assembly of two chromene derivatives: Synthesis, crystal structure, Hirshfeld surface, quantum computational and molecular docking studies, J. Mol. Struct. 1225 (2021) 129104.

[3] D.A. Uhlenheuer, K. Petkau, L. &Brunsveld, Combining supramolecular chemistry with biology, Chem. Soc. Rev. 39 (8) (2010) 2817–2826.

[4] E. Bosch, N.P. Bowling, Supramolecular Polymer Formation Featuring Cooperative Halogen Bonding and Nonconventional sp2-CH··· N Hydrogen Bonding, Cryst. Growth Des. 19 (10) (2019) 5929–5933.

[5] S. Sirimulla, J.B. Bailey, R. Vegesna, M. Narayan, Halogen interactions in protein–ligand complexes: implications of halogen bonding for rational drug design, J. Chem. Inf. Model. 53 (11) (2013) 2781–2791.

[6] F. Zordan, L. Brammer, P. Sherwood, Supramolecular Chemistry of Halogens: Complementary Features of Inorganic (M- X) and Organic (C- X ʹ) Halogens Applied to M-X...X-C Halogen Bond Formation, J. Am. Chem. Soc. 127 (16) (2005) 5979–5989.

[7] P. Metrangolo, F. Meyer, T. Pilati, G. Resnati, G. &Terraneo, Halogen bonding in supramolecular chemistry, AngewandteChemie Int. Ed. 47 (33) (2008) 6114–6127.

[8] T. Xiao, L. Zhou, X.Q. Sun, F. Huang, C. Lin, L. Wang, Supramolecular polymers fabricated by orthogonal self-assembly based on multiple hydrogen bonding and macrocyclic host–guest interactions, Chin. Chem. Lett. 31 (1) (2020) 1–9.

[9] L.C. Gilday, S.W. Robinson, T.A. Barendt, M.J. Langton, B.R. Mullaney, P.D. Beer, Halogen bonding in supramolecular chemistry, Chem. Rev. 115 (15) (2015) 7118–7195.

[10] W. Wang, Y. Zhang, W.J. &Jin, Halogen bonding in room-temperature phosphorescent materials, Coord. Chem. Rev. 404 (2020) 213107.

[11] X. Pang, H. Wang, X.R. Zhao, W.J. Jin, Co-crystallization turned on the phosphorescence of phenanthrene by C–Br··· π halogen bonding, π–hole··· π bonding and other assisting interactions, CrystEngComm 15 (14) (2013) 2722–2730.

[12] H. Yang, M.W. Wong, Application of halogen bonding to organocatalysis: a theoretical perspective, Molecules 25 (5) (2020) 1045.

[13] F. Heinen, D.L. Reinhard, E. Engelage, S.M. Huber, A Bidentate Iodine (III)-Based Halogen-Bond Donor as a Powerful Organocatalyst, AngewandteChemie Int. Ed. 60 (10) (2021) 5069–5073.

[14] Y. Lu, Y. Liu, Z. Xu, H. Li, H. Liu , W. Zhu, Halogen bonding for rational drug design and new drug discovery, Expert Opin. Drug Discov. 7 (5) (2012) 375–383.

[15] P.J. Costa, R. Nunes, D. Vila-Viçosa, Halogen bonding in halocarbon-protein complexes and computational tools for rational drug design, Expert Opin. Drug Discov. 14 (8) (2019) 805–820.

[16] B.K. Saha, A. Nangia, M. Jaskólski, Crystal engineering with hydrogen bonds and halogen bonds, CrystEngComm 7 (58) (2005) 355–358.

[17] D.M. Ivanov, N.A. Bokach, Yu. KukushkinV, A. Frontera, Metal Centers as Nucleophiles Oxymoron of Halogen Bond-Involving Crystal Engineering, Chemistry–A Eur. J. (2021).

[18] G.M. Sheldrick, A short history of SHELX, Acta Crystallogr., Sect. A: Found. Crystallogr. 64 (2008) 112–122.

[19] G.M. Sheldrick, Crystal structure refinement with SHELXL, Acta Crystallogr., Sect. C: Struct. Chem. 71 (2015) 3–8.

[20] A.L. Spek, Single-crystal structure validation with the program PLATON, J. Appl. Crystallogr. 36 (2003) 7–13.

[21] C.F. Macrae, I. Sovago, S.J. Cottrell, P.T. Galek, P. McCabe, E. Pidcock, M. Platings, G.P. Shields, J.S. Stevens, M. Towler, Mercury 4.0: from visualization to analysis, design and prediction, J. Appl. Crystallogr. 53 (2020) 226.

[22] M. Frisch, G. Trucks, H. Schlegel, G. Scuseria, M. Robb, J. Cheesemana, V. Zakrzewski, J. Montgomery, R. Stratmann, J. Burant, Gaussian 98, Revision A. 11.4, Gaussian, Inc., Pittsburgh, PA, 2002. http://www.gaussian.com/.

[23] T. Tsuneda, J.W. Song, S. Suzuki, K. &Hirao, On Koopmans' theorem in density functional theory, J. Chem. Phys. 133 (17) (2010) 174101.

[24] R. Dennington, T. Keith, J. Millam, GaussView, version 5l;, Semichem Inc., 2009.

[25] T. Lu, F. Chen, Multiwfn: a multifunctional wavefunction analyzer, J. Comp. Chem. 33 (5) (2012) 580–592.

[26] W. Humphrey, A. Dalke, K. Schulten, VMD: visual molecular dynamics, J. Mol. Graph. 14 (1) (1996) 33–38.

[27] A. Saeed, S. Ashraf, U. Flörke, Z.Y.D. Espinoza, M.F. Erben, H. Pérez, Supramolecular self-assembly of a coumarine-based acylthiourea synthon directed by π-stacking interactions: Crystal structure and Hirshfeld surface analysis, J. Mol. Struct. 1111 (2016) 76–83.

[28] A. Saeed, M. Bolte, M.F. Erben, H. Pérez, Intermolecular interactions in crystalline 1-(adamantane-1-carbonyl)-3-substituted thioureas with Hirshfeld surface analysis, CrystEngComm 17 (39) (2015) 7551–7563.

[29] A. Saeed, U. Flörke, A. Fantoni, A. Khurshid, H. Pérez, M.F. &Erben, Close insight into the nature of intermolecular interactions in dihydropyrimidine-2 (1h-thione derivatives, CrystEngComm 19 (11) (2017) 1495–1508.

[30] D. Jayatilaka, S.K. Wolff, D.J. Grimwood, J.J. McKinnon, M.A. Spackman, CrystalExplorer: a tool for displaying Hirshfeld surfaces and visualising intermolecularinteractions in molecular crystals, In Acta Crysta. A-found. 62 (2006) S90-S90.

[31] A. Ali, M. Khalid, M.F.U. Rehman, S. Haq, A. Ali, M.N. Tahir, M. Ashfaq, F. Rasool, A.A.C. Braga, Efficient synthesis, SC-XRD, and theoretical studies of O-benzenesulfonylated pyrimidines: role of noncovalent interaction influence in their supramolecular network, ACS omega 5 (25) (2020) 15115–15128.

[32] Y. Oueslati, S. Kansız, N. Dege, To.rre de la, C. Paredes, A. Llopis-Lorente, R. Martínez-Máñez, W.S. Sta, Growth, crystal structure, Hirshfeld surface analysis, DFT studies, physicochemical characterization, and cytotoxicity assays of novel organic triphosphate, J. Mol. Model. 28 (3) (2022) 1–13.

[33] K. Sarojini, H. Krishnan, C.C. Kanakam, S. Muthu, Synthesis, X-ray structural, characterization, NBO and HOMO–LUMO analysis using DFT study of 4-methyl-N-(naphthalene-1-yl) benzene sulfonamide, Spectrochim. Acta Part A 96 (2012) 657–667.

[34] S. Şahin, N. Dege, 2022. (E)-N-(3-chlorophenyl)-1-(5-nitro-2-(piperidin-1-yl) phenyl) methanimine: X-Ray, DFT, ADMET, Boiled-Egg Model, Druggability, Bioavailabilty, and Human Cyclophilin D (CypD) Inhibitory Activity, J. Mol. Struct. 1250 (2022) 131744.

[35] Sharif, S., Saeed, M., Dege, N., Bano, R., Gilani, M.A., Sahin, O., Ahmad, S. and Ch, A.R., 2021. Synthesis, Crystal Structure, Thermal, Magnetic Properties and DFT Computations of a Ytterbium (III) Complex Derived from Pyridine-2, 6-Dicarboxylic Acid.

[36] D. Avcı, S. Altürk, F. Sönmez, Ö. Tamer, A. Başoğlu, Y. Atalay, B. Zengin Kurt, N. Dege, Novel metal complexes containing 6-methylpyridine-2-carboxylic acid as potent α-glucosidase inhibitor: synthesis, crystal structures, DFT calculations, and molecular docking, Mol. Diversity 25 (1) (2021) 171–189.

[37] K.J. Pampa, C.S. Karthik, M.K. Hema, P. Mallu, N.K. Lokanath, Post-synthetic modification of supramolecular assemblies of β-diketonato Cu (II) complexes: comparing and contrasting the molecular topology by crystal structure and quantum computational studies, CrystEngComm 23 (24) (2021) 4344–4369.

[38] M. Prabhaharan, A.R. Prabakaran, S. Gunasekaran, S. Srinivasan, DFT studies on vibrational spectra, HOMO–LUMO, NBO and thermodynamic function analysis of cyanuric fluoride, Spectro chim. Acta Part A 136 (2015) 494–503.

[39] N.K. Nkungli, J.N. &Ghogomu, Theoretical analysis of the binding of iron (III) protoporphyrin IX to 4-methoxyacetophenone thiosemicarbazone via DFT-D3, MEP, QTAIM, NCI, ELF, and LOL studies, J. Mol. Model. 23 (7) (2017) 1–20.

[40] G. Saleh, C. Gatti, L. Lo Presti, J. Contreras-García, Revealing non-covalent interactions in molecular crystals through their experimental electron densities, Chemistry-A Eur. J. 18 (48) (2012) 15523.

[41] M.K. Priya, B.K. Revathi, V. Renuka, S. Sathya, P.S. &Asirvatham, Molecular structure, spectroscopic (FT-IR, FT-Raman, 13C and 1H NMR) analysis, HOMO-LUMO energies, Mulliken, MEP and thermal properties of new chalcone derivative by DFT calculation, Mater. Today: Proc. 8 (2019) 37–46.